Nuclear Materials and Energy 42 (2025) 101871

Contents lists available at ScienceDirect

Nuclear Materials and Energy

journal homepage: www.elsevier.com/locate/nme

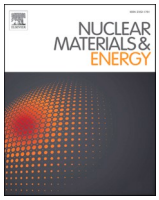

Embrittlement of chromium alloys after neutron irradiation at high temperatures to damage doses of 10–46 dpa

Vladimir Chakin [a,*], Ramil Gaisin [a], Carsten Bonnekoh [a], Michael Duerrschnabel [a], Michael Rieth [a], Bronislava Gorr [a], Mikola Brodnikikovsky [b], Mikola Krapivka [b], Sergey Firstov [b]

[a] Karlsruhe Institute of Technology (KIT), Institute for Applied Materials, P.O. Box 3640, 76021 Karlsruhe, Germany
[b] Institute for Problems in Materials Science (IPMS), Omeliana Pritsaka (Krzhizhanovsky) str., 3, 03142 Kyiv, Ukraine

ARTICLE INFO

Keywords:
Chromium alloy
Radiation embrittlement
Neutron irradiation

ABSTRACT

The study of chromium alloys, including the low-alloyed BX-2 K alloy and Cr-Fe alloys alloyed with Zr, Y, Al, Mn, Mo additions, after irradiation at temperatures ranging from 400 to 1000 °C and neutron fluences of (2.0 − 9.3) × 10^{26} m^{-2} (E > 0.1 MeV), corresponding to damage doses of 10–46 dpa, revealed a significant tendency for radiation embrittlement in all studied alloys. The tensile ductile-to-brittle transition temperature (DBTT) for these alloys increased to 250–700 °C after irradiation, while the initial DBTT was lower than room temperature. To enhance radiation embrittlement resistance, the Cr10FeZrY alloy, which exhibits a minimum DBTT of 250 °C, is recommended as a basis for further improvement of mechanical properties of Cr-Fe alloys under neutron irradiation.

1. Introduction

An important task in the nuclear and fusion reactors development is the search for advanced structural materials that can effectively withstand the effects of neutron irradiation at high operation parameters both temperature and damage dose. For example, increasing the operating temperature of the fuel element cladding of fast nuclear reactors is one of the main possibilities to increase the efficiency of the reactor [1,2].

Chromium alloys are considered as promising structural materials for nuclear reactors with higher operating temperatures compared to stainless steels [3,4]. Currently, Cr-Fe alloys (see the Cr-Fe phase diagram in Fig. 1 [5,6]) with a chromium content of up to 35 wt% have been considered for nuclear and fusion applications due to their lower swelling and activation properties compared to austenitic steels [7–9]. However, using these materials will not allow to reach a significant increase in the operating temperature.

Until now, alloys with chromium content ranging from 50 to 90 wt% have remained largely unexplored. The goal of this study is to examine how the mechanical properties of the low-alloy chromium alloy BX-2 K, and Cr-Fe alloys with 60 to 10 wt% iron, change after being exposed to high neutron doses at elevated temperatures, with a focus on the effects of irradiation on their mechanical properties. The present study compiles irradiation data on nine different chromium-based alloys over a wide temperature and irradiation dose range. The work began back in 1980-s, but the results have never been published before in a scientific paper, and they are valuable for understanding the general behavior of chromium alloys under extreme conditions.

2. Experimental

2.1. Materials, samples, heat treatments

The chemical composition of the chromium alloys is shown in Table 1 (the accuracy of the measurements is ± (20–30) %). These alloys were fabricated using an arc-melter in argon atmosphere with a non-consumable tungsten electrode. After melting, the BX-2 K alloy was hot pressed at 1000–1200 °C with a final deformation of 80–88 %, followed by polygonization annealing of the rods at 1050 °C for 0.5 h. In this case, a fine-grained structure is formed with a grain size of 5–7 μm with sub-grains measuring 0.75 μm. The Cr-Fe alloys, after melting, were hot-pressed at 1000 °C with a final deformation of about 90 %. The irradiation of all Cr-Fe alloys was performed in the deformed state. The Cr-Fe alloy specimens were cut from the rods in the direction of deformation. A characteristic feature of the deformed state is the so-called fibrous structure in the cross-section of the rod, which is characterized by the presence of fibers from 20 to 90 mm long and from 5 to 25 mm wide.

* Corresponding author.

https://doi.org/10.1016/j.nme.2025.101871
Received 12 November 2024; Received in revised form 19 December 2024; Accepted 6 January 2025
Available online 8 January 2025

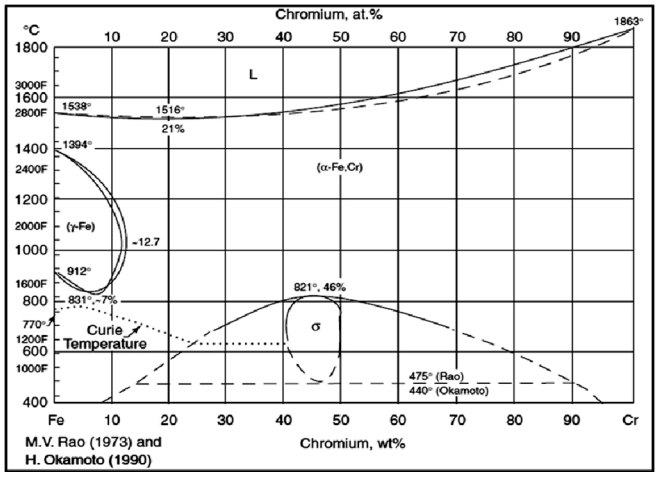

Fig. 1. The binary Fe-Cr phase diagram.

Long-term and short-term annealing of chromium alloy specimens, in place of irradiation, was conducted in a furnace under an argon atmosphere at temperatures of 750, 900, and 1200 °C.

2.2. Irradiation

Irradiation of the chromium alloy specimens was conducted in the H-1 to H-6 rigs located in 5th row of the BOR-60 research fast reactor with a sodium coolant. The specimens were placed in an inner sealed capsule made of Nb-1.1Zr-0.1C alloy, immersed in a liquid sodium environment. The irradiation temperature of the specimens was regulated by a helium-filled gap between coaxial outer and inner cylindrical capsules. The outer capsule, located in the flow of primary sodium, was made of stainless steel. Irradiation temperature and neutron fluence (the corresponding duration of irradiation t is also presented) (see Table 2) were calculated based on known values of energy release in the irradiated materials and the neutron flux in the reactor channel as well as the intensity of gamma radiation. The accuracy of the irradiation temperature calculation is ± 10 %, and for the neutron flux about 20 %. The damage dose calculation was performed according to the NRT standard for the specific placement of the specimens within the reactor channels. During irradiation, the H-4 rig was relocated to a channel further from the reactor core, resulting in a temperature drop of 100–160 °C in the specimens (see Table 2).

2.3. Mechanical tests

Radiation embrittlement of chromium alloys was assessed through tensile tests, conducted on 1236R and 1931U testing machines located in hot cells. The maximum load during tests was 1000 kg. The tests were conducted in a vacuum of up to 5×10^{-5} Torr, at temperatures ranging from room temperature to 1000 °C, with a strain rate of 8.3×10^{-4} s^{-1}. The load is measured using a strain gauge, the deformation is measured using a displacement sensor and a pair of selsyns. The margin of error for determining strength characteristics was ± 5 %, and for relative elongation, ±10 %. Microhardness was measured using the PMT-4D device (an indentation force of 0.1 kg, 5 indentations was made per specimen) with remote control, an error margin was ± 5 %. The microhardness test includes three stages: the first stage is the process of loading with a diamond pyramid lasting 20 s, the second stage is holding in the final position for 20 s, the third stage is the unloading stage lasting 20 s.

Cylindrical tensile specimens, with working part dimensions of Ø3 × 15 mm, were fabricated from the chromium alloy rods. After fabrication, the specimens were electropolished in a 50 % HNO_3 acid solution at a voltage of 15 V.

The abbreviations in Figures in Section 3 are as follows:

"init." in Figs. 2 and 3 means an initial state of BX-2 K alloy, i.e. a state before irradiation;
"ann." in Figs. 2, 3 and 8 means a state of alloys after annealing;
"init. deform." in Figs. 6-13 means an initial deformed state of alloys;
"irr." in Figs. 6-13 means a state of material after irradiation.

Table 2
Irradiation parameters of chromium alloys.

Rig	T_{irr}, °C	F, $\times 10^{26}$ m^{-2}, E > 0.1 MeV	t, h	D, dpa
H-1	400–830	4.0	7400	20
H-2	400–780	2.0	3700	10
H-3	560–800	2.4	4450	12
H-4	500–1000	6.9	12,800	35
H-5	630–750	3.8	7050	19
H-6	470–670	9.3	17,200	46

3. Results

3.1. Low-alloyed BX-2 K chromium alloy

The BX-2 K chromium alloy in its initial state before irradiation exhibits excellent tensile properties (see Fig. 2), with a favorable combination of strength (yield stress $\sigma_{0.2}$, Fig. 2a) and ductility (total relative elongation δ_0, Fig. 2b) across a temperature range from room temperature to 1000 °C. However, after annealing at 750 °C for 3500 h, the alloy shows embrittlement at temperatures up to 300 °C. Increasing the annealing temperature to 900 °C also embrittles the alloy. Only annealing at 1200 °C for 1 h results in significant softening and an increase in total relative elongation δ_0 beyond the initial state. The embrittling effect of high-temperature, long-term annealing is further intensified by neutron irradiation.

Fig. 3 shows the dependence of yield stress ($\sigma_{0.2}$) (Fig. 3a) and total relative elongation (δ_0) (Fig. 3b) of the BX-2 K alloy on testing temperature after irradiation at 600 °C to a neutron fluence of $F = 2.8 \times 10^{26}$ m^{-2}. Absolutely brittle fracture is observed up to 600 °C, with the first signs of ductility appearing at 700 °C. For consistency, we will define the tensile ductile–brittle transition temperature (DBTT) as the average temperature between these two points (i.e., the last brittle and the first ductile failures); thus, in this case, DBTT = 650 °C. A pronounced

Table 1
Chemical composition of chromium alloys in wt.%.

Alloy	Cr	Fe	Al	Mn	Mo	Zr	Y	La	Ta	V	C	O	N	H
BX-2 K	base							0.32	0.26	0.4	0.006	0.05	0.01	<0.001
Cr Fe10ZrY	–	10				0.2	0.2				0.002	0.02	0.01	–
Cr Fe35ZrY	–	35				0.2	0.2				0.005	0.025	0.025	–
Cr Fe35AlZrY	–	35	3			0.2	0.5				0.004	0.03	0.016	–
Cr Fe35AlMnY	–	35	0.9	0.05			<0.1				0.008	0.03	0.016	–
Cr Fe35MoY	–	35			0.5		0.5				0.011	0.021	0.021	–
Cr Fe50	–	50									0.012	0.01	0.01	–
Cr Fe60ZrY	–	60				0.1	0.15				0.015	0.02	0.02	–
Cr Fe60AlZrY	–	60	4.7			0.2	0.06				0.02	0.02	0.018	–

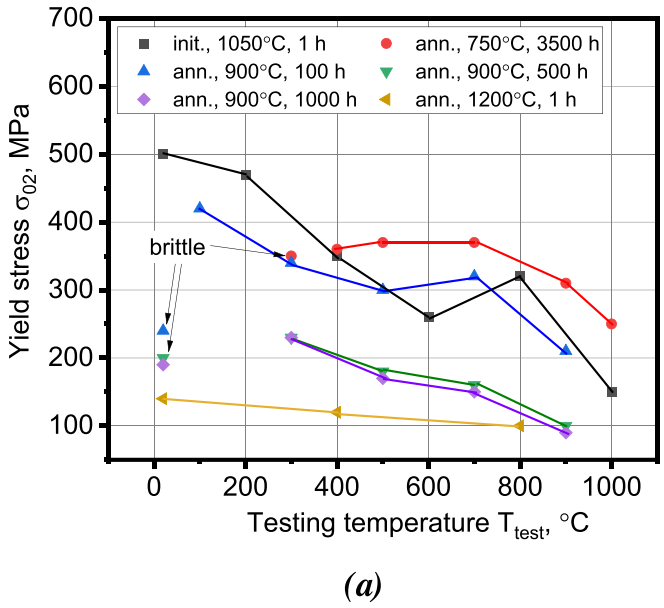

Fig. 2. Yield stress $\sigma_{0.2}$ (a) and total relative elongation δ_0 (b) of BX-2 K alloy on testing temperature T_{test} after annealing at 750, 900 and 1200 °C.

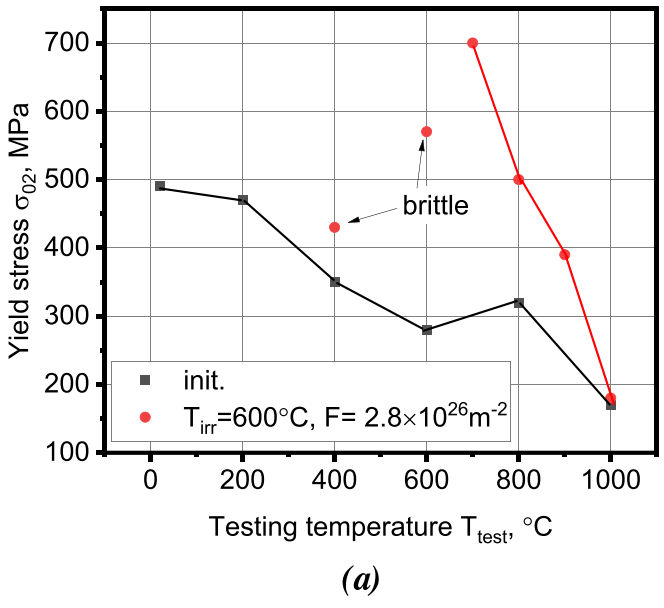

Fig. 3. Yield stress $\sigma_{0.2}$ (a) and total relative elongation δ_0 (b) of BX-2 K alloy on testing temperature T_{test} after irradiation at T_{irr} = 600 °C up to neutron fluence F = 2.8 × 10^{26}m^{-2}.

increase in yield strength ($\sigma_{0.2}$) is also observed at temperatures above the DBTT.

A summary of the irradiation effects on the tensile properties of the BX-2 K alloy is shown in Fig. 4. Here, radiation hardening is defined as $\Delta\sigma_{0.2} = \sigma_{0.2irr} - \sigma_{0.2init}$ (Fig. 4a), where $\sigma_{0.2irr}$ is the yield stress after irradiation and $\sigma_{0.2init}$ is the yield stress in the initial state before irradiation. For microhardness, radiation hardening is represented by $\Delta H_\mu = H_{\mu irr} - H_{\mu init}$ (Fig. 4b), where $H_{\mu irr}$ is the microhardness after irradiation and $H_{\mu init}$ is the microhardness in the initial state before irradiation. Fig. 4c shows the temperature dependence of the DBTT. All three parameters show a sharp decrease up to 700 °C. At temperatures above 700 °C, there is an increase in these parameters, followed by a decrease for both $\Delta\sigma_{0.2}$ and DBTT.

A dependence of radiation hardening ($\Delta\sigma_{0.2}$, above), microhardness (ΔH_μ, middle), and DBTT (below) of the BX-2 K alloy on neutron fluence (F) for irradiation temperatures of 650–750 °C is presented in Fig. 5. A monotonic increase in both radiation hardening $\Delta\sigma_{0.2}$ (Fig. 5a) and DBTT (Fig. 5c) occurs with increasing neutron fluence, although the growth rate slows as the maximum neutron fluence value is approached. The radiation hardening ΔH_μ (Fig. 5b) demonstrates a linear increase on increasing neutron fluence.

The $\Delta\sigma_{0.2}$ on F dependence can be fitted by an exponential relationship:

$$\Delta\sigma_{0.2} = (539 \pm 80) - (1666 \pm 1182) \times \exp((-0.8 \pm 0.4) \times F), \quad (1)$$

The ΔH_μ on F dependence can be fitted by a linear relationship:

$$\Delta H_\mu = (1579 \pm 55) \times (65 \pm 11) \times F, \quad (2)$$

The DBTT on F dependence can be fitted by an exponential relationship:

$$DBTT = (450 \pm 19) - (661 \pm 159) \times \exp((-0.6 \pm 0.1) \times F), \quad (3)$$

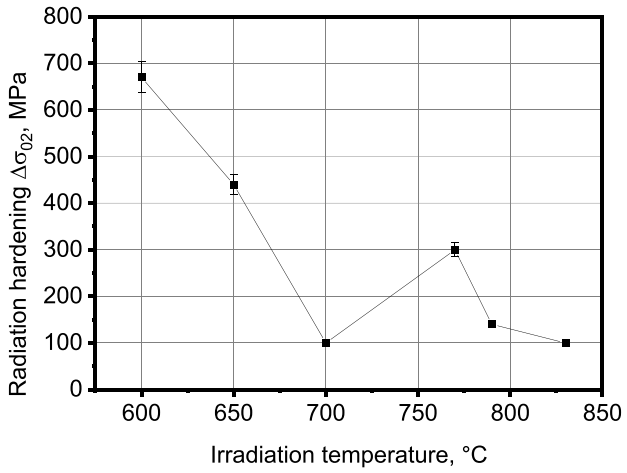

(a)

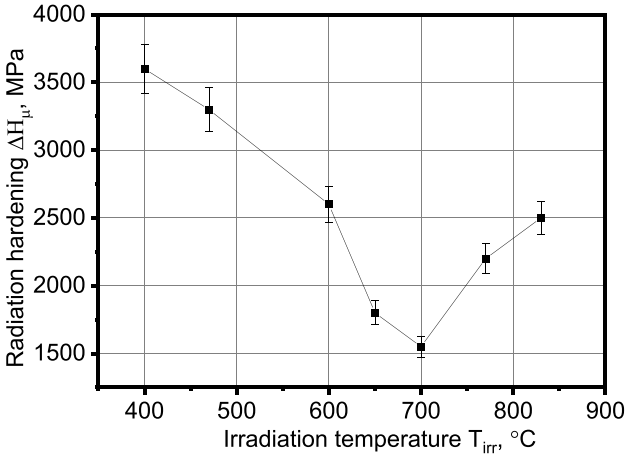

(b)

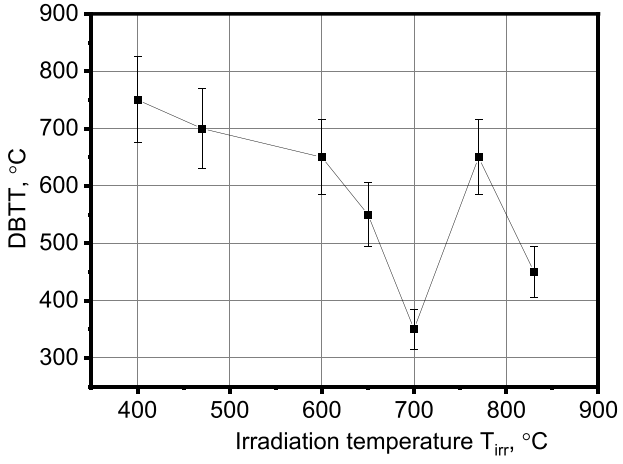

(c)

Fig. 4. Radiation hardening $\Delta\sigma_{0.2}$ (a), ΔH_μ (b) and DBTT (c) of BX-2 K alloy on irradiation temperature T_{irr}, normalized to neutron fluence F= (2.8–3.2) × 10^{26} m^{-2}, $T_{test} = T_{irr}$.

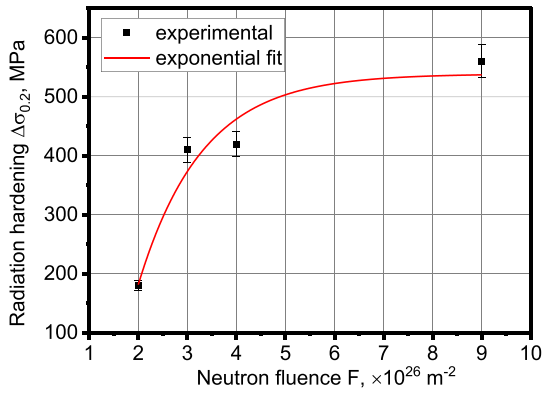

The $\Delta\sigma_{0.2}$ on F dependence can be fitted by an exponential relationship:

$$\Delta\sigma_{0.2} = (539\pm80) - (1666\pm1182) \times \exp((-0.8\pm0.4) \times F), (1).$$

(a)

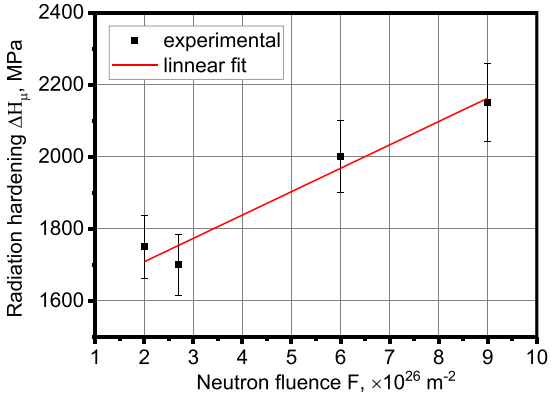

The ΔH_μ on F dependence can be fitted by a linear relationship:

$$\Delta H_\mu = (1579\pm55) \times (65\pm11) \times F, \quad (2).$$

(b)

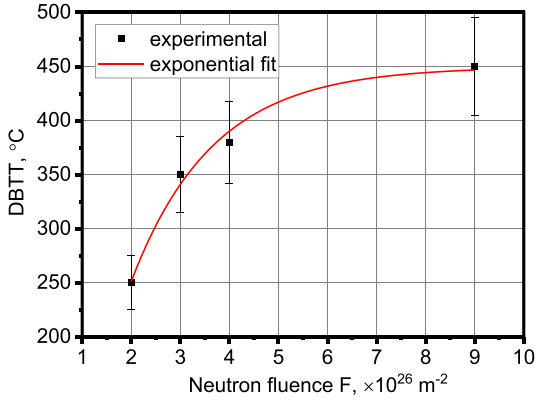

The DBTT on F dependence can be fitted by an exponential relationship:

$$DBTT = (450\pm19) - (661\pm159) \times \exp((-0.6\pm0.1) \times F), (3).$$

(c)

Fig. 5. Radiation hardening $\Delta\sigma_{0.2}$ (a), ΔH_μ (b) and DBTT (c) of BX-2 K alloy on neutron fluence F for irradiation temperatures T_{irr} = 650–750 °C ($T_{test} = T_{irr}$).

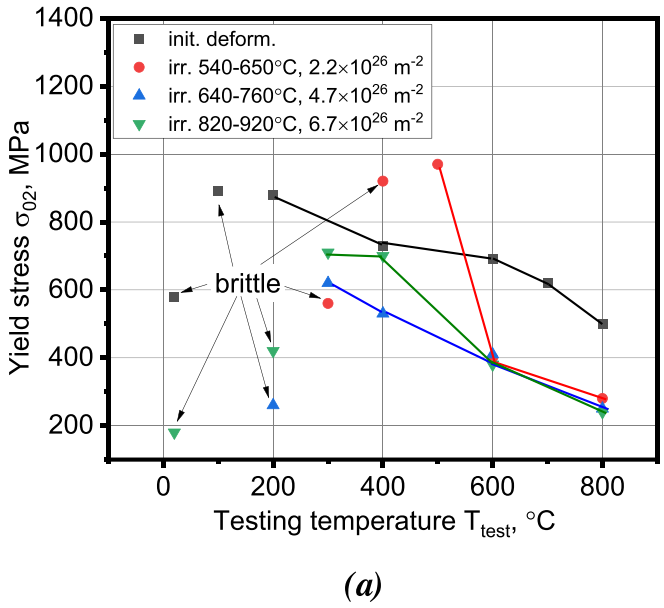

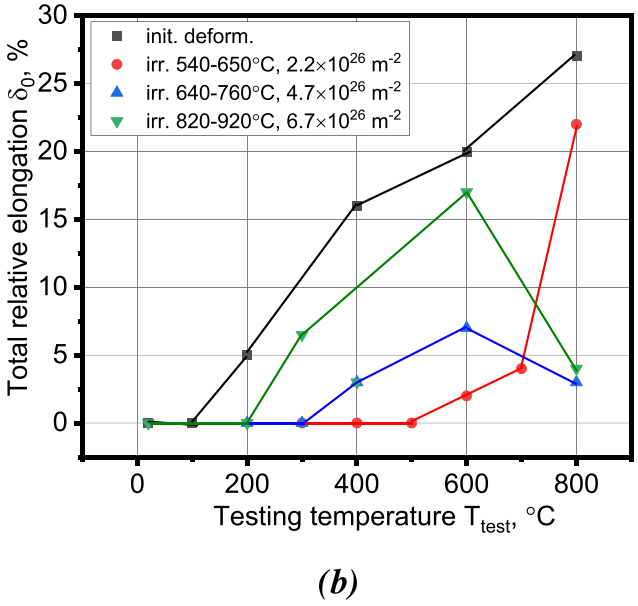

Fig. 6. Yield stress $\sigma_{0.2}$ (a) and total relative elongation δ_0 (b) of Cr Fe10ZrY alloy on testing temperature T_{test} after irradiation at T_{irr} = 540–920 °C up to neutron fluence F= (2.2–6.7) × 10^{26} m^{-2}.

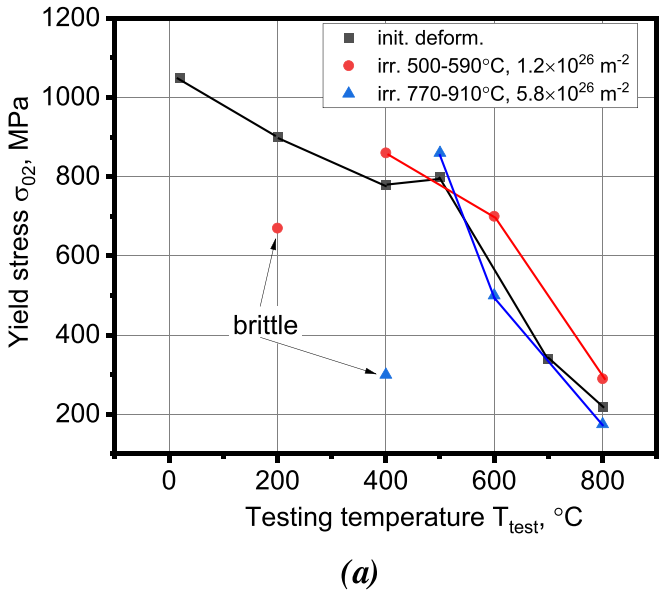

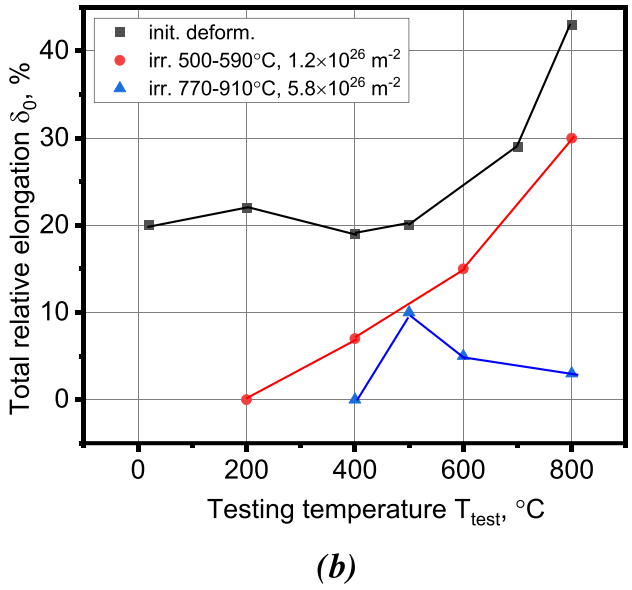

Fig. 7. Yield stress $\sigma_{0.2}$ (a) and total relative elongation δ_0 (b) of Cr Fe35ZrY alloy on testing temperature T_{test} after irradiation at T_{irr} = 500–910 °C up to neutron fluence F= (1.2–5.8) × 10^{26} m^{-2}.

3.2. Cr-Fe alloys with Zr and Y additions

Figs. 6, 7, and 9 display the yield stress ($\sigma_{0.2}$) and total relative elongation (δ_0) values of Cr-Fe alloys with small additions of Zr and Y, as a function of testing temperature after irradiation across a wide range of temperatures and neutron fluences. Fig. 8 presents the same mechanical characteristics for the Cr Fe50 alloy. These chromium alloys exhibit varying degrees of radiation hardening and embrittlement effects depending on the irradiation parameters. The most severe embrittlement was observed in the Cr Fe50 alloy without additional alloying with Zr and Y. In this alloy, embrittlement occurs even without irradiation, after annealing at 700 °C for 1000 h, leading to an increase in DBTT to 450 °C (see Fig. 6b).

Table 3 summarizes data from Figs. 6-9 regarding the radiation-induced evolution of the ductile–brittle transition temperature (DBTT) in Cr-Fe alloys (with Zr and Y). The lowest DBTT values are observed for the Cr Fe10ZrY alloy after irradiation at temperatures between 640 and 920 °C.

3.3. Cr Fe35 and Cr Fe60 alloys with Al, Mn, Mo additions

Figs. 10 and 11 display the yield stress ($\sigma_{0.2}$) and total relative elongation (δ_0) of two Cr FeZrY alloys with Al additions as a function of testing temperature after irradiation at high temperatures. The Cr Fe35AlZrY and Cr Fe60AlZrY alloys exhibit radiation-induced embrittlement at temperatures up to 400 °C (Fig. 10b) and 200 °C (Fig. 11b) and softening, beginning at 500°C (Fig. 10a) and 400 °C (Fig. 11a), respectively.

Replacing Zr with Mn (see Fig. 12) in the Cr Fe35AlZrY alloy (Fig. 10) results in reduced brittleness, with DBTT values ranging from 450 to 350 °C (Fig. 12b), and leads to radiation hardening instead of softening (Fig. 12a). Conversely, replacing Zr with Mo (see Fig. 13) in the Cr Fe35ZrY alloy (Fig. 7) results in increased brittleness (Fig. 13b), with

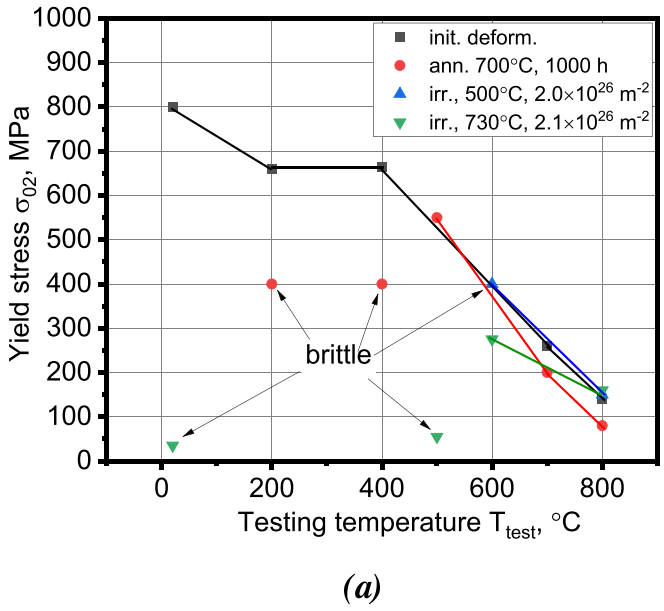

Fig. 8. Yield stress $\sigma_{0.2}$ (a) and total relative elongation δ_0 (b) of Cr Fe50 alloy on testing temperature T_{test} after annealing at 700 °C for 1000 h and irradiation at T_{irr} = 730 °C up to neutron fluence F = 2.1 × 10^{26} m^{-2}.

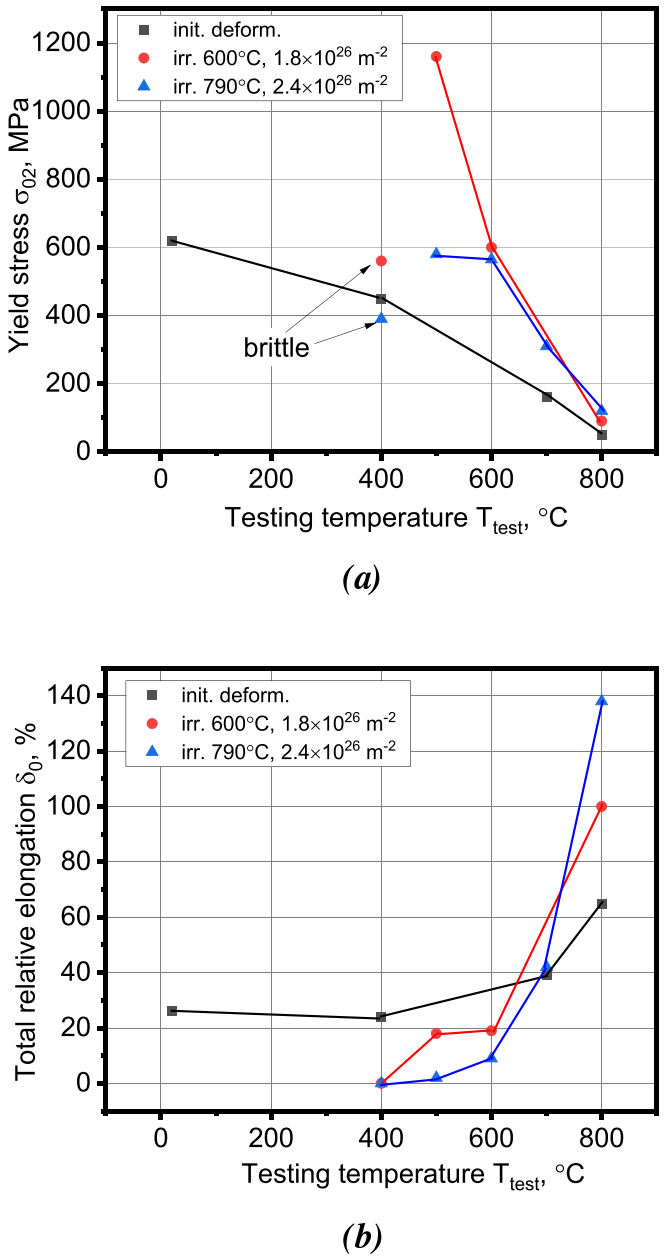

Fig. 9. Yield stress $\sigma_{0.2}$ (a) and total relative elongation δ_0 (b) of Cr Fe60ZrY alloy on testing temperature T_{test} after irradiation at T_{irr} = 600–790 °C up to neutron fluence F= (1.8–2.4) × 10^{26} m^{-2}.

DBTT values ranging from 450 to 700 °C, while maintaining the softening effect (Fig. 13a).

Table 4 summarizes data from Figs. 10-13 regarding the DBTT values of Cr-Fe alloys (with Al, Mn, and Mo). The lowest DBTT is observed for Cr Fe60AlZrY at 250 °C, while the highest DBTT is found in Cr Fe35MoY at 700 °C.

4. Discussion

As indicated by the results of the mechanical tests presented in Section 3, all the investigated chromium alloys exhibited a tendency toward significant embrittlement after irradiation. However, a closer examination of the results reveals certain chromium alloys that embrittled to a comparatively lesser extent. Therefore, it is worthwhile to explore the reasons behind the differences in the susceptibility of chromium alloys to radiation embrittlement, particularly in relation to variations in alloying elements.

Neutron irradiation can influence the degree of embrittlement in chromium alloys in two primary ways: by creating radiation defects in the structure, such as clusters, dislocation loops, and vacancy voids [10], or, specifically for alloys in the binary Cr-Fe system, by forming and evolving the σ-phase, which is known for its high brittleness and low so-called brittle strength [11–13]. The presence of brittle σ-phase particles in the microstructure of irradiated Cr-Fe alloys significantly contributes to the embrittlement of these materials [13].

Refractory body-centered cubic (BCC) metals such as molybdenum and tungsten in the Group VIA family, which includes chromium, as well as alloys based on these metals, exhibit a pronounced tendency toward low-temperature radiation embrittlement (LTRE) after irradiation [14–17]. The ferritic-martensitic low-activation steel EUROFER97 (an RAFM-type steel), which also has a BCC lattice structure, shows a similar tendency toward LTRE following irradiation [18–20]. In irradiated

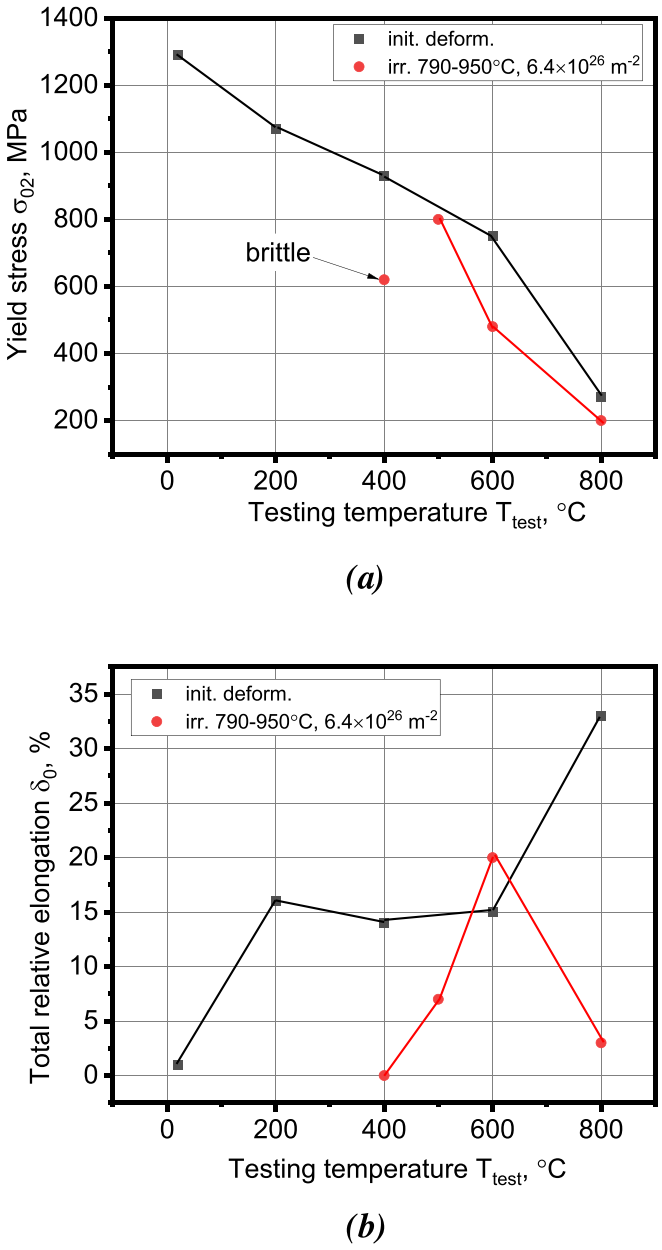

Fig. 10. Yield stress $\sigma_{0.2}$ (a) and total relative elongation δ_0 (b) of Cr Fe35AlZrY alloy on testing temperature T_{test} after irradiation at T_{irr} = 740 °C up to neutron fluence F = 2.2 × 10^{26}m^{-2}.

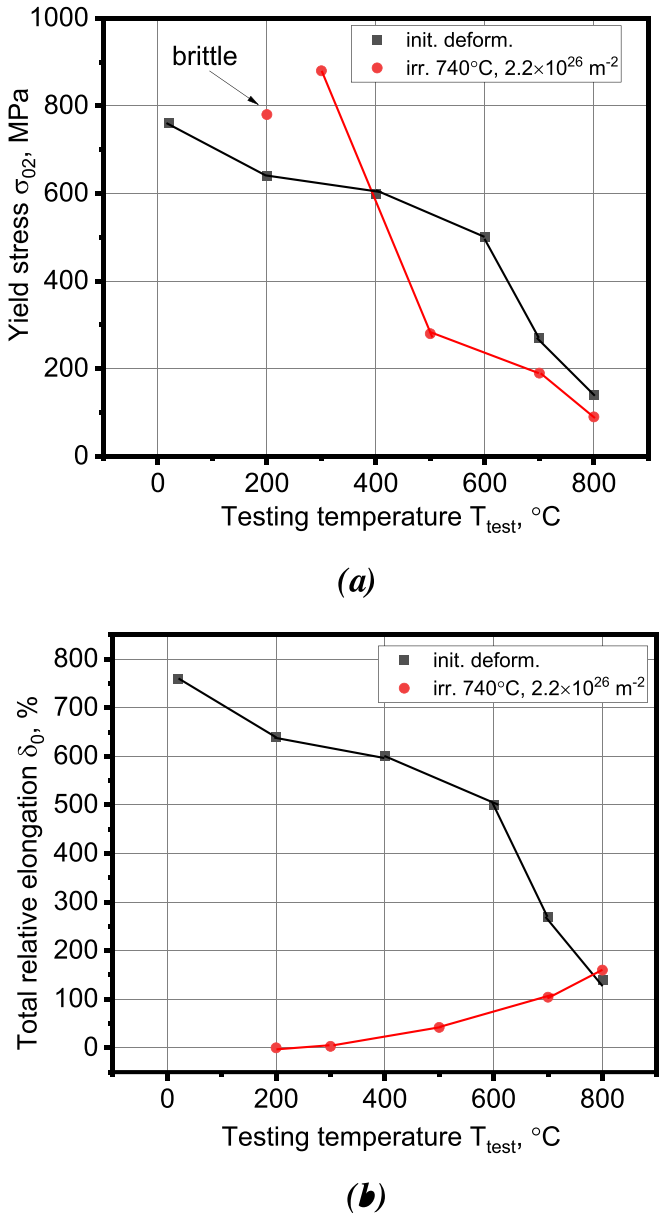

Fig. 11. Yield stress $\sigma_{0.2}$ (a) and total relative elongation δ_0 (b) of Cr Fe60AlZrY alloy on testing temperature T_{test} after irradiation at T_{irr}= (790–950) °C up to neutron fluence F = 6.4 × 10^{26}m^{-2}.

tungsten, high-density dislocation loops and voids develop within the microstructure. Additionally, the segregation of transmuted Re and Os atoms at dislocation loops eventually leads to the formation of χ-phase precipitates on these loops [21,22]. This radiation-induced evolution of the tungsten microstructure results in significant radiation hardening, accompanied by a shift of the ductile-to-brittle transition temperature (DBTT) to higher temperatures. For EUROFER97 steel irradiated at 300–335 °C up to 70 dpa, nearly homogeneous dislocation loops form throughout the steel matrix. These radiation-induced dislocation loops are considered the primary contributors to irradiation hardening and embrittlement [23,24].

Let us consider the radiation-induced changes in the microstructure of the low-alloyed BX-2 K chromium alloy [10]. The initial state of the alloy is characterized by a structure with a sub-grain size of 0.75 μm, a density of free dislocations of 10^{15} m^{-2}, and second phases with particle sizes of 100 nm. At an irradiation temperature of 670 °C and a neutron fluence of 1.8 × 10^{26} m^{-2}, vacancy pores form with sizes ranging from 6 to 8 nm and a density of 2.5 × 10^{22} m^{-3}. The average cell size increases to 1.4 μm, accompanied by the formation of denuded zones free of any radiation defects, dislocations and precipitates along the grain boundaries and sub-grain boundaries, measuring 10 to 15 nm in width. Additionally, dislocations with a density of 10^{10} to 10^{11} m^{-2} are present in the structure of the irradiated BX-2 K alloy. The results of microstructural studies by TEM are not included in Section 3, but they are partly present in the references [10–13] therefore, they are presented here for the discussion of the results of mechanical tests.

The presence of voids contributes to an increase in the strength of the alloy, resulting in radiation hardening, as the voids serve as effective barriers to dislocation motion during deformation. Estimates indicate that the DBTT of the BX-2 K chromium alloy after irradiation increases proportionally with the increase in radiation hardening ($\Delta\sigma_{0.2}$) (see Fig. 14).

The DBTT on $\Delta\sigma_{0.2}$ dependence can be fitted by a linear relationship:

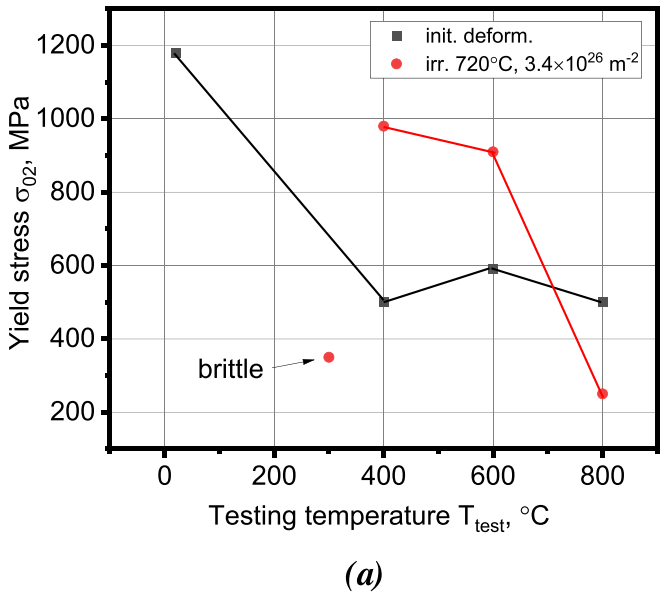

Fig. 12. Yield stress $\sigma_{0.2}$ (a) and total relative elongation δ_0 (b) of Cr Fe35AlMnY alloy on testing temperature T_{test} after irradiation at $T_{irr} = 720$ °C up to neutron fluence $F = 3.4 \times 10^{26} m^{-2}$.

$$DBTT = (312 \pm 76) \times (1 \pm 0.3) \times \Delta\sigma_{0.2}, \quad (4)$$

Enrichment of structural sinks with iron has been observed in the Cr Fe35ZrY alloy [12,13]. After irradiation at 750 °C to a neutron fluence of 3.8×10^{26} m^{-2}, the enrichment reached 40 % of the initial content of Fe atoms. This phenomenon occurs due to the radiation-induced segregation [25,26] of Fe atoms to the outer surface, grain boundaries, and other structural sinks of point defects in Cr-Fe alloys under irradiation. The enrichment effect of these sinks leads to the formation of the σ-phase even in Cr-Fe alloys where, according to the Cr-Fe phase diagram (see Fig. 1), the σ-phase should not be present or should occur only in smaller quantities at a given alloy composition or temperature [11].

For instance, in the Cr Fe10ZrY alloy, after irradiation at temperatures between 640 and 760 °C to a neutron fluence of 4.7×10^{26} m^{-2}, small amounts of σ-phase were detected (about 0.1 % relative to the Cr Fe50 alloy, which exhibited approximately 90 % σ-phase content). This alloy also showed voids measuring 10–15 nm in size with a density of 7.9×10^{21} m^{-3} and dislocation loops measuring 15–120 nm with a density of 1.06×10^{22} m^{-3} [11].

In [12], a relationship was proposed for determining the shift of the tensile DBTT of chromium alloys under neutron irradiation:

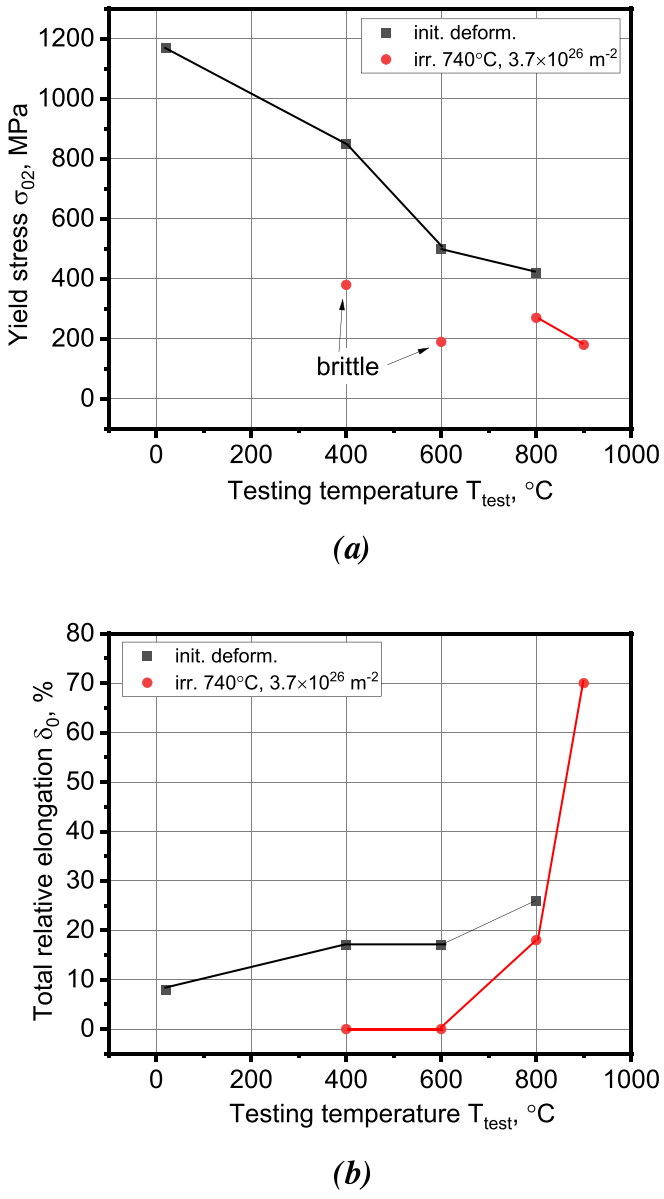

Fig. 13. Yield stress $\sigma_{0.2}$ (a) and total relative elongation δ_0 (b) of Cr Fe35MoY alloy on testing temperature T_{test} after irradiation at $T_{irr} = 740$ °C up to neutron fluence $F = 3.7 \times 10^{26} m^{-2}$.

Table 3
Influence of neutron irradiation to the DBTT of Cr FeZrY alloys.

Alloy	T_{irr}, C°	F,×10^{26} m^{-2}	DBTT, °C
Cr Fe10ZrY	540–650	2.2	450
	640–760	4.7	250
	820–920	6.7	250
Cr Fe35ZrY	500–590	1.2	300
	770–910	5.8	450
Cr Fe50	500	2.0	700
	730	2.1	550
Cr Fe60ZrY	600	1.8	450
	790	2.4	450

Table 4
Influence of neutron irradiation to the DBTT of Cr FeY alloys with additions of Al, Mn, Mo.

Alloy	T_{irr}, C°	F,×10^{26} m^{-2}	DBTT, °C
Cr Fe35AlZrY	740	2.2	450
Cr Fe60AlZrY	790–950	6.4	250
Cr Fe35AlMnY	720	3.4	350
Cr Mo35Y	740	3.7	700

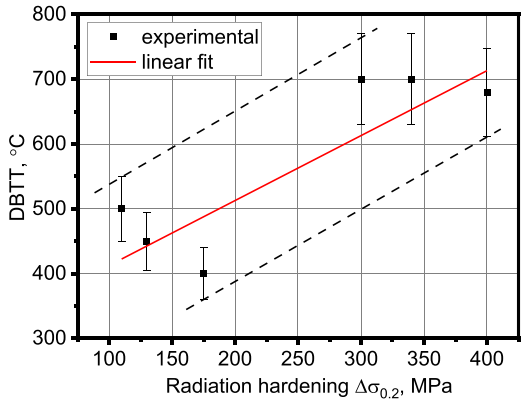

The DBTT on $\Delta\sigma_{0.2}$ dependence can be fitted by a linear relationship:
DBTT = (312±76) × (1±0.3) × $\Delta\sigma_{0.2}$,

Fig. 14. Dependence of DBTT of BX-2 K chromium alloy on radiation hardening $\Delta\sigma_{0.2} = \sigma_{0.2\ irr} - \sigma_{0.2\ init}$ for irradiation temperatures of T_{irr} = 500–800C and neutron fluences of F = (1–4) × 10^{26} m^{-2}.

$$\Delta DBTT = \Delta DBTT_{rd} + \Delta DBTT_{\sigma} = A \times (Nd)^{1/2} + B \times M_{\sigma}, \quad (5)$$

where $\Delta DBTT_{rd}$ is the shift due to the radiation defects formation;

$\Delta DBTT_{\sigma}$ is the shift due to the σ-phase formation;
N, cm^{-3} is the density of the radiation defects (voids, dislocation loops);
d, nm is the diameter of the radiation defects;
M_{σ}, is the amount of σ-phase according to the results of the X-ray phase analysis;
A, B are constants.

The relationship (5) can only provide a qualitative explanation for the observed radiation embrittlement of chromium alloys. However, low-alloyed chromium alloys lack the second term, meaning the contribution to the shift value is solely due to radiation hardening resulting from the formation of radiation defects, such as voids or dislocation loops, and lack of the σ-phase impact.

In Cr-Fe alloys, the primary factor influencing embrittlement is the amount of σ-phase present in the alloy; that is, as more σ-phase is formed, the degree of embrittlement increases. Table 5 shows the results of σ-phase amount measurements in the irradiated Cr-Fe alloys [11–13].

Table 5
Influence of neutron irradiation on σ-phase formation measured by X-ray phase analysis in Cr-Fe alloys.

Alloy	T_{irr}, C°	F,×10^{26} m^{-2}	σ-phase amount, relative unit
Cr Fe10lZrY	640–760	4.7	0.001
Cr Fe35lZrY	770–910	5.8	0.07
Cr Fe35AlZrY	740	2.2	0
Cr Fe35AlMnY	750	3.8	0
Cr Fe35MoY	740	3.7	0.08
Cr Fe50	730	2.1	0.9
Cr Fe60ZrY	790	2.4	0.07
Cr Fe60AlZrY	790–950	6.4	0

Among the studied Cr-Fe alloys, only the Cr Fe10ZrY alloy exhibited both factors—radiation defects and small σ-phase particles [11]. This alloy demonstrated the least susceptibility to radiation embrittlement, with a DBTT of 250 °C (see Table 3). This is attributed to the minimal contribution of σ-phase particles to embrittlement (see Table 5) and, consequently, the limited effect of voids and dislocation loops on radiation hardening (see Figs. 6 and 14).

Similarly, the Cr Fe60AlZrY alloy also exhibited minimal embrittlement, with a DBTT of 250 °C (see Table 4). In this alloy, no σ-phase particles were detected after irradiation, in contrast to the Cr Fe60ZrY alloy, where σ-phase particles were identified (see Table 5), ranging in size from 0.1 to 25 μm with a density of not more than 5 × 10^{9} m^{-3} [11]. This observation suggests that alloying with aluminum suppresses the formation of σ-phase in Cr-Fe alloys. Also, according to [27], the Cr-Fe-Al ternary phase diagram shows the absence of the σ-phase in the Cr Fe60AlZrY alloy at the given temperatures.

The greatest susceptibility to radiation embrittlement, aside from the low-alloyed BX-2 K alloy, was exhibited by the Cr Fe50 alloy, which has a DBTT of 700 °C (see Table 3). The microstructure of this alloy contains large σ-phase particles, and it is nearly single-phase in composition [12,13] (see Table 5). Additionally, the Cr Fe35MoY alloy, which also features large σ-phase particles in its microstructure [11] (see Table 5), demonstrated significant radiation embrittlement. This indicates that the addition of molybdenum to Cr-Fe alloys promotes the formation of σ-phase under irradiation. Moreover, according to [28], the Cr-Fe-Mo ternary phase diagram shows the presence of the σ-phase in this alloy at these irradiation temperatures.

The role of manganese in suppressing σ-phase formation is less clear, as aluminum is also present in the Cr Fe35AlMnY alloy (see Fig. 12, Table 4). However, according to [29], the Cr-Fe-Mn ternary phase diagram indicates the absence of σ-phase in this alloy at the given temperatures. This suggests that the combined individual effects of aluminum and manganese, which both reduce the tendency of Cr-Fe alloys to form σ-phase (see Table 5), contribute to increased resistance to radiation embrittlement.

A detailed analysis of previous studies on the radiation damage in chromium alloys has revealed behavior similar to that of other refractory metals and alloys, particularly their susceptibility to severe radiation embrittlement. However, there remains potential to enhance the radiation embrittlement resistance of chromium alloys through further alloy optimization, beginning with Cr-Fe alloys containing approximately 10 % Fe. Additionally, given chromium's excellent combination of physical and mechanical properties—especially its inherent heat resistance and high corrosion resistance in aggressive environments—the development of chromium alloys for use in aircraft engine turbines and other industrial applications is currently under consideration [30].

5. Conclusions

A study was conducted on the susceptibility of the low-alloyed BX-2 K chromium alloy and chromium-iron alloys alloyed with Zr, Y, Al, Mn, and Mo to radiation embrittlement after irradiation at temperatures ranging from 400 to 1000 °C to neutron fluences of (2.0 − 9.3) × 10^{26} m^{-2} (E > 0.1 MeV), corresponding to damage doses of 10–46 dpa.

All chromium alloys exhibited a tendency toward radiation embrittlement, with the tensile ductile-to-brittle transition temperature (DBTT) shift ranging from 250 to 700 °C. The smallest DBTT shift (250 °C) was observed in the Cr Fe10ZrY and Cr Fe60AlZrY alloys, while the largest DBTT shift (700 °C) was found in the Cr50Fe and Cr Fe35MoY alloys. The remaining alloys displayed intermediate susceptibility to radiation embrittlement.

In the Cr-Fe alloys, a positive effect of alloying with aluminum and manganese, was observed regarding their tendency to embrittlement

under irradiation. In contrast, alloying with molybdenum had a negative effect, leading to increased embrittlement.

Further improvement in the radiation embrittlement resistance of Cr-Fe alloys may be achieved by refining and optimizing additional alloying strategies for chromium alloys with an iron content of 5 to 15 wt%.

CRediT authorship contribution statement

Vladimir Chakin: Writing – review & editing, Writing – original draft, Methodology, Investigation, Formal analysis, Conceptualization. **Ramil Gaisin:** Writing – review & editing, Methodology, Formal analysis. **Carsten Bonnekoh:** Writing – review & editing, Visualization, Software, Methodology, Formal analysis. **Michael Duerrschnabel:** Writing – review & editing, Software, Methodology, Formal analysis. **Michael Rieth:** Writing – review & editing, Software, Methodology, Formal analysis. **Bronislava Gorr:** Writing – review & editing, Supervision, Project administration, Funding acquisition, Conceptualization. **Mikola Brodnikikovsky:** Writing – review & editing, Methodology, Investigation, Formal analysis, Conceptualization. **Mikola Krapivka:** Writing – review & editing, Methodology, Investigation, Formal analysis, Conceptualization. **Sergey Firstov:** Writing – review & editing, Resources, Project administration, Methodology, Conceptualization.

Declaration of competing interest

The authors declare the following financial interests/personal relationships which may be considered as potential competing interests: Vladimir Chakin reports article publishing charges was provided by Karlsruhe Institute of Technology. Vladimir Chakin reports a relationship with Karlsruhe Institute of Technology that includes: employment. If there are other authors, they declare that they have no known competing financial interests or personal relationships that could have appeared to influence the work reported in this paper.

Acknowledgements

We would like to express our sincere gratitude to the staff of the Research Institute of Atomic Reactors for their organization of the irradiation and post-irradiation examinations of these materials, as well as for the insightful and fruitful discussions regarding the results obtained in this study.

Data availability

No data was used for the research described in the article.

References

[1] A.D. Perez-Valseca, G. Espinosa-Paredes, C.G. Aguilar-Madera, E.C. Herrera-Hernandez, A.M. Gomez-Torres, Upscaling and downscaling the heat transfer process coupled with neutronic reflected core for sodium-cooled fast nuclear reactor, Int. J. Heat Mass Transf. 189 (2022) 122713.
[2] Y. Dai, X. Zheng, P. Ding, Review on sodium corrosion evolution of nuclear-grade 316 stainless steel for sodium-cooled fast reactor applications, Nucl. Eng. Technol. 53 (11) (2021) 3474–3490.
[3] A. Hishinuma, S. Isozaki, S. Takaki, K. Abiko, Attractive Characteristics of High-Chromium Iron-Based Alloys for Nuclear Reactor Application, Phys. Stat. Sol. (a) 160 (1997) 431–440.
[4] K. Suganuma, H. Kayano, S. Yajima, Mechanical properties changes of Fe-Cr alloys by fast neutron irradiation, J. Nucl. Mater. 105 (1982) 23–35.
[5] H. Okamato, Binary Alloy Phase Diagrams, 2nd ed.,, ASM International, 1990.
[6] Bandar AL-Mangour,, Powder Metallurgy of Stainless Steel: State-Of-The Art, Challenges, and Development. Chapter 2 in: Stainless Steel, Nova Science Publishers, Inc., 2015.
[7] H. Kim, J.G. Gigax, J. Fan, F.A. Garner, T.-L. Sham, Lin Shao, Swelling resistance of advanced austenitic alloy A709 and its comparison with 316 stainless steel at high damage levels, J. Nucl. Mater. 527 (2019) 151818.
[8] A.M. Dvoriashin, S.I. Porollo, Y.V. Konobeev, F.A. Garner, Influence of high dose neutron irradiation on microstructure of EP-450 ferritic–martensitic steel irradiated in three Russian fast reactors, J. Nucl. Mater. 329–333 (2004) 319–323.
[9] T. Muroga, T. Nagasaka, Y. Li, H. Abe, S. Ukai, A. Kimura, T. Okuda, Fabrication and characterization of reference 9Cr and 12Cr-ODS low activation ferritic/martensitic steels, Fusion Eng. Des. 89 (2014) 1717–1722.
[10] V.P. Chakin, V.A. Kazakov, Radiation resistance of low-alloyed chromium alloys, Preprint RIAR-7 (790), ZNIIatominform, Moscow, 1990 in Russian.
[11] V.P. Chakin, V.A. Kazakov, Z.E. Ostrovsky, Yu.D. Goncharenko, B.A. Mochalov, V. F. Pushkin, V.A. Trubachev, Radiation resistance of chromium-iron alloys, Preprint RIAR-7 (834), Dimitrovgrad, 1992, in Russian.
[12] V.P. Chakin, V.A. Kazakov, Z.E. Ostrovsky, Yu.D. Goncharenko, Behavior of sigma-phase under neutron irradiation of chromium-iron alloys, Preprint RIAR-21 (824), Dimitrovgrad, 1991, in Russian.
[13] V. Chakin, V. Kazakov, Yu. Goncharenko, Z. Ostrovsky, Formation of the σ-phase in Cr-Fe alloys under irradiation, J. Nucl. Mater. 233–237 (1996) 573–576.
[14] L.V. Gorynin, V.A. Ignatov, V.V. Rybin, S.A. Fabritsiev, V.A. Kazakov, V.P. Chakin, V.A. Tsykanov, V.R. Barabash, Y.G. Prokofyev, Effects of neutron irradiation on properties of refractory metals, J. Nucl. Mater. 191–194 (1992) 421–425.
[15] S.A. Fabritsiev, V.A. Gosudarenkova, V.A. Potapova, V.V. Rybin, L.S. Kosachev, V. P. Chakin, A.S. Pokrovsky, V.R. Barabash, Effects of neutron irradiation on physical and mechanical properties of Mo-Re alloys, J. Nucl. Mater. 191–194 (1992) 426–429.
[16] R.G. Abernethy, J.-S.-K.-L. Gibson, A. Giannattasio, J.D. Murphy, O. Wouters, S. Bradnam, L.W. Packer, M.R. Gilbert, M. Klimenkov, M. Rieth, H.-C. Schneider, C. D. Hardie, S.G. Roberts, D.E.J. Armstrong, Effects of neutron irradiation on the brittle to ductile transition in single crystal tungsten, J. Nucl. Mater. 527 (2019) 151799.
[17] A. Zinovev, D. Terentyev, C.-C. Chang, C. Yin, A. Bakaev, M. Rieth, P. Lied, J. Reiser, C. Bonnekoh, Effect of neutron irradiation on ductility of tungsten foils developed for tungsten-copper laminates, Nucl. Mater. Energy 30 (2022) 101133.
[18] C. Bob van der Schaaf, Y.D. Petersen, J.W. Carlan, E. Rensman, X.A. Gaganidze, High dose, up to 80 dpa, mechanical properties of Eurofer 97, J. Nucl. Mater. 386–388 (2009) 236–240.
[19] M. Klimenkov, U. Jäntsch, M. Rieth, A. Moeslang, Correlation of microstructural and mechanical properties of neutron irradiated EUROFER97 steel, J. Nucl. Mater. 538 (2020) 152231.
[20] O. Kachko, A. Puype, D. Terentyev, C.-C. Chang, M. Rieth, R.H. Petrov, Impact of neutron irradiation on the tensile properties of advanced EUROFER97-type steels, J. Nucl. Mater. 599 (2024) 155176.
[21] M. Klimenkov, M. Dürrschnabel, U. Jäntsch, P. Lied, M. Rieth, H.C. Schneider, D. Terentyev, W. Van Renterghem, Microstructural analysis of W irradiated at different temperatures, J. Nucl. Mater. 572 (2022) 154018.
[22] M. Klimenkov, U. Jäntsch, M. Rieth, H.C. Schneider, D. Terentyev, W. Van Renterghem, Influence of transmutation-induced Re/Os content on defect evolution in neutron-irradiated W, J. Nucl. Mater. 592 (2024) 154950.
[23] M. Klimenkov, U. Jäntsch, M. Rieth, M. Dürrschnabel, A. Möslang, H.C. Schneider, Post-irradiation microstructural examination of EUROFER-ODS steel irradiated at 300 °C and 400 °C, J. Nucl. Mater. 557 (2021) 153259.
[24] E. Gaganidze, C. Petersen, E. Materna-Morris, C. Dethloff, O.J. Weiß, J. Aktaa, A. Povstyanko, A. Fedoseev, O. Makarov, V. Prokhorov, Mechanical properties and TEM examination of RAFM steels irradiated up to 70 dpa in BOR-60, J. Nucl. Mater. 417 (2011) 93–98.
[25] R.A. Johnson, N.Q. Lam, Solute segregation under irradiation, J. Nucl. Mater. 69–70 (1978) 424.
[26] N.Q. Lam, P.R. Okamoto, H. Wiedersich, Effects of solute segregation and precipitation on void swelling in irradiated alloys, J. Nucl. Mater. 74 (1978) 101.
[27] K. Korniyenko, L. Dreval, Al-Cr-Fe Ternary Phase Diagram Evaluation, MSI, Materials Science International Services GmbH, Stuttgart, 2022, p. 4, 10.14873.4.3.
[28] A. Kroupa, Cr-Fe-Mo Ternary Phase Diagram Evaluation, MSI, Materials Science International Services GmbH, Stuttgart, 2007, p. 1, 10.15307.1.4M3.
[29] J. Vrestal, Cr-Fe-Mn Ternary Phase Diagram Evaluation, MSI, Materials Science International Services GmbH, Stuttgart, 2007, p. 1, 10.11754.1.9.
[30] Kan Ma, Thomas Blackburn, Johan P. Magnussen, Michael Kerbstadt, Pedro A. Ferreirós, Tatu Pinoma, Christina Hofer, David G. Hopkinson, Sarah J. Day, Paul A.J. Bagot, Michael P. Moody, Mathias C. Galetz, Alexander J. Knowles, Chromium-based bcc-superalloys strengthened by iron supplements, Acta Materialia (2023) 257119183.